Title

PHOTCOISSOCIATION OF 1,2-CHLOROIODOETHANE AT 248 AND 266 nm; THE ENTHALPY OF FORMATION OF CH2ClCH2I

Author

Minton, T.K.

Publication Date

1984-04-01

LBL-17535
Preprint

Lawrence Berkeley Laboratory
UNIVERSITY OF CALIFORNIA

Materials & Molecular Research Division

Submitted to the Journal of Chemical Physics

PHOTODISSOCIATION OF 1,2-CHLOROIODOETHANE AT 248 AND 266 nm; THE ENTHALPY OF FORMATION OF CH_2ClCH_2I

T.K. Minton, P. Felder, R.J. Brudzynski, and Y.T. Lee

April 1984

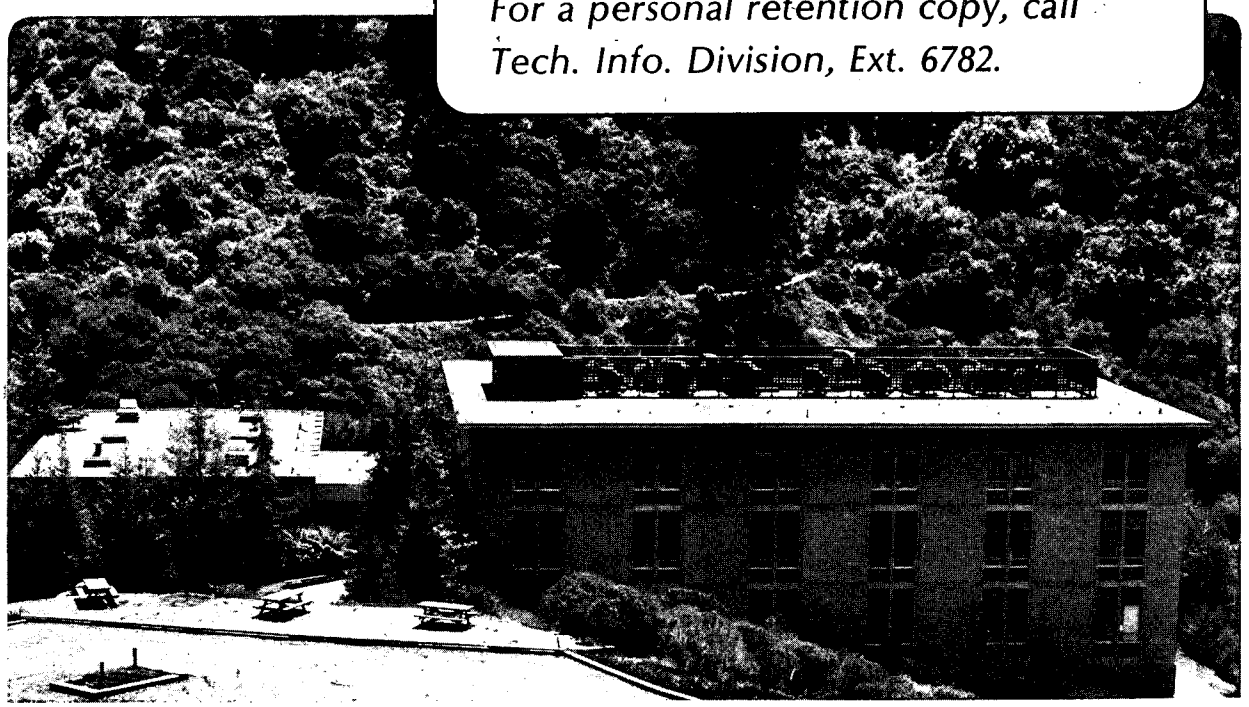

Prepared for the U.S. Department of Energy under Contract DE-AC03-76SF00098

DISCLAIMER

LBL-17535

Photodissociation of 1,2-chloroiodoethane at 248 and 266 nm; the enthalpy of formation of CH_2ClCH_2I

Timothy K. Minton, Peter Felder, Richard J. Brudzynski, and Yuan T. Lee

Materials and Molecular Research Division
Lawrence Berkeley Laboratory and
Department of Chemistry, University of California
Berkeley, California 94720 USA

This work was supported by the Director, Office of Energy Research, Office of Basic Energy Sciences, Chemical Sciences Division of the U.S. Department of Energy under Contract No. DE-AC03-76SF00098.

Photodissociation of 1,2-chloroiodoethane at 248 and 266 nm; the enthalpy of formation of CH_2ClCH_2I

Timothy K. Minton, Peter Felder, Richard J. Brudzynski, and Yuan T. Lee

Materials and Molecular Research Division
Lawrence Berkeley Laboratory and
Department of Chemistry, University of California
Berkeley, California 94720 USA

ABSTRACT

The technique of photofragmentation translational spectroscopy has been utilized to study the photodissociation of CH_2ClCH_2I at excitation wavelengths of 248 and 266 nm. The primary photofragments are C_2H_4Cl and either $I^*(^2P_{1/2})$ or $I(^2P_{3/2})$. A fraction of the chloroethyl radical product contains enough internal excitation after the primary process to undergo secondary dissociation into C_2H_4 and Cl. By observing the threshold for this secondary process, the reaction enthalpy for $CH_2ClCH_2I \rightarrow C_2H_4 + Cl + I$ was determined, which leads to: $\Delta H^o_{f,0}(CH_2ClCH_2I) = -7.8 \pm 1$ kcal/mole. The c.m. translational energy distribution of the photofragments was derived for both the I^* and I channels, yielding I^*/I branching ratios of 1.5 at 248 nm and 3 at 266 nm. The translational energy distribution also revealed that about 50% of the excess energy went into translation. The angular distributions of dissociation products with respect to the laser polarization indicate that the primary photodissociation process for the ground and excited state iodine channels at both wavelengths proceeds via a parallel transition - that is, the transition moment must be nearly parallel to the C-I bond.

I. INTRODUCTION

Excitation of the alkyl iodides in the 200-300 nm region of the spectrum leads to transitions of a non-bonding $5p_\pi$ iodine electron to a σ^* molecular orbital,[1c,d] which is seen as the familiar $n \rightarrow \sigma^*$ continuum.[2] It has long been known[3-6] that the photodissociation of alkyl halides in this region yields two states of atomic iodine:

$$RI + h\nu \rightarrow \begin{cases} R^\cdot + I^*(^2P_{1/2}) \\ R^\cdot + I(^2P_{3/2}) \end{cases} \qquad (1)$$

For small RI, the major pathway is toward formation of the spin-orbit excited state $^2P_{1/2}$ of iodine (which we will denote I^*). This phenomenon has led to the development of the iodine laser.[4]

Photofragmentation translational spectroscopy studies[7-12] have shown that following the $n \rightarrow \sigma^*$ absorption, dissociation proceeds directly along the repulsive surface, with a large fraction of the excess energy released in translation. For example, in CH_3I, the fraction of excess energy appearing in translation is approximately 0.85, and in C_2H_5I, this fraction is ~0.60. Even in fluorinated alkyl iodides,[10,11] such as C_2F_5I and C_2F_4BrI, in which lower frequency vibrations and larger exit impact parameters could result in excitation of more fragment vibrational and rotational degrees of freedom, about 50% of the excess energy appears in translation. From the anisotropy in the product angular distributions, it is seen that the lifetime of the excited state must be less than one rotational

period. Dzvonik, Yang, and Bersohn[7] made a careful study of the anisotropy in the broadband photodissociation of CH_3I and concluded that the lifetime after absorption of a photon was 0.07 psec.

The anisotropy of the product angular distributions with respect to the polarization of the laser also provides information regarding the orientation of the transition moment of the $n \rightarrow \sigma^*$ transition. According to the molecular orbital theory of Mulliken,[1] the $n \rightarrow \sigma^*$ continuum is composed of three overlapping bands, which arise from transitions from the ground N state to the ^1Q, $^3Q_1$, and $^3Q_0$ states. The $N \rightarrow {}^3Q_0$ transition should be polarized parallel to the C-I bond and should correlate to formation of I^*, while the $N \rightarrow {}^1Q$ and $N \rightarrow {}^3Q_1$ transitions should be polarized perpendicular to the C-I bond and should correlate to formation of ground state I. For the diatomics, I_2 and HI, Mulliken's predictions have been borne out by experiment.[12,13] However, in the case of the alkyl iodides, both I and I^* are observed to occur via parallel transitions at 266 nm,[8] suggesting that curve crossing is important. The underlying structure of the $n \rightarrow \sigma^*$ continuum for CH_3I has been probed with magnetic circular dichroism (MCD),[14] but even with this information, the relative yields of I^* and I at a particular wavelength cannot be predicted because of the complication of curve crossing.

Due to interest in the iodine laser, the quantum yields of I^* from photodissociation of alkyl iodides have received considerable attention, but despite all the effort spent, disagreement abounds even in the ubiquitous methyl iodide studies. Table I shows various I^* quantum yields reported for CH_3I at 266 and 248 nm. The most reliable values in the table should be the results obtained by photofragmentation translational spectroscopy at 266 nm. This method, based on the pioneering work of Wilson and co-

workers,[8,15-17] utilizes the fact that the products from the I^* channel recoil slower than the products from the I channel, and it is ideal because it yields an absolute ratio of I^* and I atoms. Consistent with the photofragmentation spectroscopy results at 266 nm is the value of Hunter, Lunt, and Kristjansson[18] who used an optoacoustic technique. But at 248 nm, none of the experiments agree. In a recent study using laser induced VUV fluorescence,[19] I^* quantum yields at 248 nm for many alkyl iodides were reported. The drawback of this study is that the average of the values from refs. 20 and 21 for CH_3I was used as a calibration standard. Clearly, the wide range of reported I^* quantum yields for CH_3I make it a rather tenuous standard. I^* quantum yields from UV photolysis of alkyl iodides certainly require further investigation.

The energetics of the dissociation of CH_2ClCH_2I resulting from an $n \rightarrow \sigma^*$ transition present many interesting features for a photofragment translational spectroscopy study. For example, the photon energy at an excitation wavelength of 266 nm is 107.5 kcal/mole, but only about 55 kcal/mole of energy is needed to break the C-I bond, leaving ~52 kcal/mole excess energy. If electronically excited I^* is formed, this excess energy is reduced by 21.7 kcal/mole to ~30 kcal/mole. The C-Cl bond energy in the C_2H_4Cl fragment has been estimated to be only about 20 kcal/mole, so unless a substantial fraction of the excess energy is carried away in translation, the internal energy in the chloroethyl fragment will exceed the C-Cl dissociation limit. If about 50% of the excess energy appears in translation, as has been seen in other iodoethanes,[10,11] then the photodissociation channel leading to formation of ground state I is likely to result in complete secondary dissociation of the C_2H_4Cl fragment into

C_2H_4 and Cl, while the channel leading to I^* might leave only a fraction of the chloroethyl radicals with enough internal energy to dissociate.

In the primary photodissociation process of 1,2-chloroiodoethane, the momentum of the system must be conserved. Accordingly, the C_2H_4Cl and I fragments will move with opposite directions in the center of mass coordinate system as shown schematically in Fig. 1. As the total energy of the system is also conserved, the smaller the recoil velocity, or kinetic energy, the larger the internal energy of the alkyl fragment. If the internal excitation of the C_2H_4Cl radical exceeds the C-Cl bond dissociation energy, then the radical will dissociate and will be depleted from the C_2H_4Cl velocity (or time-of-flight) distribution. The minimum translational energy of stable C_2H_4Cl corresponds to production of C_2H_4 + Cl with zero kinetic energy and no internal excitation. Consequently, by determining the minimum in the total translational energy distribution for all fragments that leads to stable chloroethyl radicals, the energy required to break both the C-I and C-Cl bonds in 1,2-chloroiodoethane can be determined, from which the heat of formation ΔH_f^o of CH_2ClCH_2I can be estimated.

As Fig. 1 illustrates, if we measure the velocity (or time-of-flight) distribution of one fragment, we can derive the energetics for the whole system by using conservation of energy and momentum. Detection of iodine will yield the total translational energy distribution, $P(E_T)$, of the primary photodissociation products for both I^* and I channels, but if we observe the stable C_2H_4Cl fragment, the range of the $P(E_T)$ distribution which we derive and the knowledge of the C-Cl bond dissociation energy in the C_2H_4Cl radical will allow the identification of the iodine electronic state that is associated with the production of stable chloroethyl radicals. As will be

seen, stable C_2H_4Cl product correlates only with I^* formation because ground state I does not carry away enough energy to stabilize the chloroethyl product. Thus, the measurement of both the C_2H_4Cl and I fragments makes it possible to discriminate between the $P(E_T)$ distributions for the I^* and I channels, allowing the I^*/I branching ratio to be deduced.

From angular and time-of-flight distributions at both 248 and 266 nm, the polarization dependence of the photodissociation processes can be derived, permitting a comparison of the excitation of two different parts of the $n \rightarrow \sigma^*$ continuum and revealing the relation between the initial excitation and the extent of subsequent curve crossing.

In addition to our interest in the detailed dynamics of the photofragmentation of CH_2ClCH_2I, we wished to test the possibility of producing a molecular beam of cold C_2H_4Cl radicals by photodissociation. If stable C_2H_4Cl radicals can be prepared by crossing a pulsed supersonic molecular beam with a UV laser just outside the nozzle, the radicals produced in the high density region will be confined in the beam, and after being cooled in the expansion, they will survive unperturbed.

This beam of 2-chloroethyl radicals could then be used for a time resolved experiment which would directly probe the time scale of the intramolecular energy transfer from a locally excited C-H overtone stretching mode to other vibrational degrees of freedom by the measurement of the dissociation lifetime. The C_2H_4Cl radical would be an ideal system to study for the following reasons. First, as the C-Cl bond is fairly weak, only four quanta of C-H stretch (i.e., excitation of the third overtone) are needed to reach well above the dissociation limit. Second, the predicted RRKM lifetime of

C_2H_4Cl when excited to the third overtone is on the order of a few picoseconds. Thus, if the intramolecular relaxation from the local excitation of the C-H stretching modes to other modes is slower than a few picoseconds, then the experimental dissociation lifetime would provide a good measure of the rate of intramolecular energy transfer. Finally, there is more than one C-H stretching mode accessible, allowing the rates of two different intramolecular relaxation processes to be compared.

II. EXPERIMENT

The apparatus used was a universal crossed molecular beam machine[22] in which an ultraviolet laser was substituted for one of the molecular beams (see Fig. 2). The resulting configuration was a supersonic molecular beam of CH_2ClCH_2I (custom synthesized by Fairfield Chemical, Fairfield, SC) which was crossed at right angles by the UV laser. Photodissociation products were detected in the plane of the laser and molecular beams by a rotatable mass spectometer. The flight path length from the interaction region to the ionizer was 20.8 cm. Two different lasers were used in order to study the photodissociation of 1,2-chloroiodoethane at both 248 and 266 nm.

In both experiments, the molecular beam was formed by bubbling a carrier gas through liquid CH_2ClCH_2I which was held at 20°C (vapor press. = 7 torr) and then expanding the mixture through a 0.005 in. (0.12 mm) dia. nickel nozzle. The nozzle was heated at the tip to prevent cluster formation. The molecular beam passed through three stages of differential pumping before it reached the main chamber where it intersected the laser. A skimmer was used to define the beam to an angular divergence of 2°. The distance from the nozzle to the interaction region was about 9.5 cm.

For the 248 nm experiment, an unpolarized Lambda Physik EMG 101 laser was used on the KrF transition at a repetition rate of 40 Hz. The average pulse energy was ~125 mJ. Two optics were used to focus the laser. A 50 cm fl MgF_2 cylindrical lens oriented to focus the beam horizontally was followed immediately by a 35 cm fl UV-grade fused silica spherical lens, giving a final spot size of 2.2 mm wide and 4.5 mm high in the interaction region. The CH_2ClCH_2I was seeded in He at a total stagnation pressure of 700

torr (1% CH_2ClCH_2I/99% He) and the nozzle temperature was 130°C, yielding a peak velocity of 1770 m/sec with a velocity spread (FWHM) of 9%.

For the 266 nm experiment, the fourth harmonic of a Quanta Ray DCR-1 Nd:YAG laser was used. The output was polarized horizontally – that is, in the plane of the molecular beam and detector. A Quanta Ray Harmonic Generator, Model HG-2, was used to generate the fourth harmonic. The output from the harmonic generator passed through a Pellin-Broca prism after which the unwanted first and second harmonics were directed into a beam dump. The fourth harmonic went directly from the prism into the machine through a 50 cm fl UV-grade fused silica spherical lens. The final spot diameter at the interaction region was 2.8 mm. Average pulse energies were ~30 mJ. The molecular beam conditions for the experiment at this wavelength differed from those at 248 nm in that Ar was used as the carrier gas and the stagnation pressure was 400 torr (1.8% CH_2ClCH_2I/98.2% Ar). Also, the nozzle was heated to 228°C. The resulting beam had a peak velocity of 707.8 m/sec with an aveage velocity spread of 8.4%.

The molecular beam velocity distributions were determined by fitting time-of-flight (TOF) measurements on the beam to an assumed form for the velocity distribution, $N(v) \propto v^2 \exp[-(\frac{v}{\alpha} - S)^2]$, (see refs. 10 and 23). The TOF measurements were obtained differently for the two experiments. At 266 nm, the usual method of a "single-shot" slotted disk was employed to chop the beam. However, at 248 nm, a holeburning method was used. In holeburning, the detector is positioned along the molecular beam axis and tuned to the parent mass. Molecules photodissociated by a laser pulse scatter off axis and give rise to a hole in the TOF. The shape of the

hole registered at the ionizer contains the information about the velocity distribution. In this way, the velocity distribution can be measured at any point during the experiment without insertion of the slotted disk. The disadvantage of holeburning is that the signal-to-noise ratio is much worse than in the conventional slotted disk method.

At 248 nm, TOF measurements were made at detector angles from 5° to 30°. Signal was detected at m/e = 127, 63, 35, and 26, corresponding to I^+, $C_2H_4Cl^+$, Cl^+, and $C_2H_2^+$, respectively. The respective counts/laser pulse at 10° were 1.95, 0.02, 0.72, and 0.67. Due to the fragmentation of C_2H_4Cl in the ionizer and the high mass 28 background in the detector, masses 63 and 28 were not suitable for monitoring the chloroethyl product, but mass 26 proved to be an acceptable mass for this purpose. Mass 35 (Cl^+) was not used for monitoring C_2H_4Cl because most of the mass 35 signal was found to arise from Cl atoms. Typical counting durations were 20,000 laser pulses for I^+ and 500,000 pulses for $C_2H_2^+$.

At 266 nm, TOF measurements were made at detector angles from 7° to 35°. Signal was detected at m/e = 127(I^+) and 26($C_2H_2^+$). The mass 26 TOF was only taken at 7°, where we observed ~0.04 counts/pulse of signal. Mass 127 at 10° gave ~0.98 counts/pulse. Mass 26 was counted for 176,000 pulses, while the mass 127 TOF's were counted for 40,000 pulses.

It should be noted that the two experiments reported here were performed six months apart. The change to different experimental conditions was suggested from the analysis of the first experiment (at 248 nm).

III. RESULTS AND ANALYSIS

The experimental data with which we derive the center of mass product translational energy distribution $P(E_T)$ and the c.m. angular distribution $w(\theta)$ for the photodissociation products are the TOF distributions $N(t)$ and the laboratory angular distributions $N(\Theta)$. For a single photon dipole transition, the c.m. angular distribution of the fragments must have the form,[17b]

$$w(\theta) = \frac{1}{4\pi}[1 + \beta P_2(\cos\theta)], \qquad (2)$$

where θ is the angle between the electric vector of the laser light and the c.m. recoil direction of the products. β is the anisotropy parameter and must lie in the range $-1 \leq \beta \leq 2$. The $P(E_T)$ and β are determined by comparing calculated TOF and angular distributions with the experimental data. The calculated distributions are obtained by assuming a $P(E_T)$ distribution and a value for β and then convoluting them with the beam velocity distribution, ionizer length, and other apparatus effects. By varying the $P(E_T)$ and β, the best simultaneous fits to all the data are obtained.

It should be noted that the TOF distributions show the total time for a fragment to go from the interaction region to the ionizer, and after ionization, through the quadrupole mass spectrometer to the Daly-type ion counter. The true TOF from the interaction region to the ionizer is given by subtracting the relatively short ion flight time (typically <5% of the total flight time) from the measured TOF. The ion flight time for a singly charged ion of mass m has been estimated experimentally, and it can be expressed in μsec by the formula $\alpha\sqrt{m}$ where the parameter α is a function of ion energy and other spectrometer parameters and is equal to 1.80 for the 248 nm experiment and 1.94 for the 266 nm experiment.

A. TOF and angular distributions

Fig. 3 shows the TOF data along with the best fits at various laboratory angles for the iodine fragment at 266 nm. Two components in the TOF are definitely apparent. Similar effects have been observed in other alkyl iodides[8,9] where the fast component is attributed to formation of ground state $I(^2P_{3/2})$ while the slow component is ascribed to the formation of the spin-orbit excited state $I^*(^2P_{1/2})$.

In the case of the TOF data at 248 nm (Fig. 4), the fast shoulder is not so obvious partly because the translational energy distributions for products leading to ground and excited state iodine are not as separated as they are at 266 nm (see part B) and also because the molecular beam velocity in the 248 nm experiment was more than twice that in the 266 nm experiment, yielding poorer time resolution.

The effect of the molecular beam velocity as well as the reason for the observation of two different peaks in the 248 nm TOF can be seen by considering the experiment in terms of the kinematic diagram shown in Fig. 5. The vertical arrow is the molecular beam velocity vector. The center of mass is at the tip of this vector. An arrow from the c.m. to one of the circles represents the velocity that a particular recoiling fragment has in the c.m. coordinate system after photodissociation. The angle between this c.m. fragment velocity vector and the line on which the molecular beam velocity vector lies is the c.m. angle θ of the product. The angle between the molecular beam velocity vector and the laboratory velocity vector of the product is the laboratory angle Θ. We detect products at a particular Θ, and we can see a peak in the TOF spectrum at an arrival time corresponding to the velocity vector $\underset{\sim}{V}_{lab}$ which intersects the most probable c.m. product velocty as shown by the Newton circle. The TOF spectrum is weighted

by the transformation Jacobian from velocity to time. As can be seen, a slower beam velocity would mean better angular and temporal resolution for a given recoil velocity distribution. In addition, slight offsets in the timing of the experiment are less important with the slower beam.

There are advantages to the fast beam velocity, however. First, the signal is higher because the products are concentrated in a smaller laboratory angular range. Second, in the case where we see the "forward" and "backward" peaks in the TOF, as in the 248 nm data, we are sampling two different c.m. angles for each laboratory angle, making the fit to the TOF distribution very sensitive to the anisotropy parameter β.

The angular distributions $N(\theta)$ for the I fragment are shown in Figs. 6 and 7 for 266 and 248 nm, respectively. The 266 nm distribution is fit quite nicely by $\beta = 1.8$. However, $\beta = 1.8$ did not fit the 248 nm angular distribution well. In fact, $\beta = 2.0$ gives a better fit, but the TOF distributions at 248 nm gave the most consistent fits for $\beta = 1.8$. The poor fit in the angular distribution is attributed to a possible systematic error in the determination of the laboratory angle. An error of 0.5° in θ, which could arise from a combination of a slight misalignment of the laser and molecular beams as well as the uncertainty in the detector position, would account for the observed effect. Nevertheless, this error will not materially affect the conclusions of the experiment.

As mentioned in Section II, we observed the chloroethyl fragment at m/e = 26. The total TOF distribution for mass 26 at 248 nm (Fig. 8) exhibits an interesting feature. There is a large "spike" superimposed on a broad background. This background arises from secondary dissociation of the C_2H_4Cl into C_2H_4 and Cl, while the spike is the TOF distribution of

the chloroethyl radical which survives. Fig. 9 shows a blow-up of the spike with the best fit. The mass 26 TOF at 266 nm (Fig. 10) did not show a broad background partly because of the relatively poor signal-to-noise ratio, but mainly because of the fact that a large fraction of the C_2H_4Cl product survives. In both mass 26 TOF distributions, shaded areas are shown with the best fit, illustrating the range of uncertainty in the fits to the slow side.

Another mass which was considered for observing the chloroethyl fragment was mass 35(Cl^+), whose TOF is shown in Fig. 11. While the TOF does show evidence of a peak at ~82 μsec corresponding to the stable C_2H_4Cl fragment, it certainly does not exhibit the definite spike seen in the mass 26 TOF. Thus, most of the Cl^+ ions arise from Cl atoms rather than C_2H_4Cl.

B. Product translational energy distributions

The fits to the TOF and angular distributions were calculated using the $P(E_T)$ distributions shown in Fig. 12. Because photodissociation can lead either to $I^*(^2P_{1/2})$ or $I(^2P_{3/2})$ product, the total $P(E_T)$ is the sum of two distributions. The energetics of the photodissociation process enable us to determine the ground and excited state components of the total $P(E_T)$.

A representation of the energetics is shown in Fig. 13. The energy available for translation and internal excitation of the products (E_{avl} for production of I or E^*_{avl} for production of I^*) is given by the energy conservation expressions,

$$Eavl = h\nu + E^P_{int} - D^o_o(C\text{-}I) = E_T + E^R_{int} \qquad (3)$$

$$E^*_{avl} = E_{avl} - E_{so}$$

where E^P_{int} is the internal energy of the CH_2ClCH_2I parent, which is almost negligible, and E^R_{int} is the internal energy of the C_2H_4Cl fragment after photodissociation. $D^o_o(C\text{-}I)$ for CH_2ClCH_2I is estimated to be 55.3 ± 1 kcal/mole (see Discussion). The photon energy $h\nu$ is 115 kcal/mole at 248 nm and 107.5 kcal/mole at 266 nm. E_{so} is the 21.7 kcal/mole spin-orbit splitting between I and I^*.

The minimum internal energy of the chloroethyl fragment (E^R_{int}) when ground state I is formed is given by subtracting the observed maximum E_T from the available energy (E_{avl}). At 248 nm, this minimum E^R_{int} is 21.8 kcal/mole, and at 266 nm, it is 19.0 kcal/mole. These energies are expected to be near or above the C-Cl dissociation limit for the C_2H_4Cl radical.[24] Hence, all ground state I formation should lead to secondary dissociation of the C_2H_4Cl fragment. The $P(E_T)$ derived from the fit to the mass 26 TOF should then reflect only the formation of I^*. Thus, subtracting this $P(E_T)$ for I^* formation from the total $P(E_T)$ will give the $P(E_T)$ for ground state I formation.

A complication in the reasoning above (but an important feature in this experiment) occurs because the effect of secondary dissociation is also seen in the $P(E_T)$ for I^* formation. At both wavelengths, particularly at 248 nm, even when I^* is formed, some of the C_2H_4Cl radicals have more than enough internal energy to break the C-Cl bond. Consequently, the low translational energy (high E^R_{int}) side of the $P(E_T)$ derived from the mass 26 TOF is "chopped off" relative to the total $P(E_T)$. The minimum translational energy

that the C_2H_4Cl radical is observed to have is ~15 kcal/mole at 248 nm and ~9.3 kcal/mole at 266 nm. From Eq. (3), the total energy required for the dissociation of both the iodine and the chlorine from CH_2ClCH_2I can be determined [assuming E^P_{int} is equal to zero (see Discussion)] as follows:

$$D^o_o(CH_2ClCH_2\text{-}I) + D^o_o(C_2H_4\text{-}Cl) = h\nu - E_{so} - E_T(min) \qquad (4)$$

where $D^o_o(C_2H_4\text{-}Cl)$ has been replaced for $E^R_{int}(max)$. This sum of dissociation energies is just the change in enthalpy ΔH at 0 K for the reaction,

$$CH_2ClCH_2I \rightarrow CH_2{=}CH_2 + I + Cl. \qquad (5)$$

We observe $\Delta H = 78.3 \pm 1$ kcal/mole in the 248 nm experiment and $\Delta H = 76.5 \pm 1$ kcal/mole in the 266 nm experiment. The disagreement between these two values will be considered in the following section.

From the areas under the $P(E_T)$ distributions, we can estimate a branching ratio for the formation of I^* to I. At 248 nm, $I^*/I = 1.5$, while at 266 nm, $I^*/I = 3$. These results can be compared with observations for C_2H_5I. Ref. 19 obtains $I^*/I = 2.1$ at 248 nm, while ref. 8 estimates $I^*/I \cong 3$ at 266 nm. Our results do contain some uncertainty. Because the ionization cross section in the ionizer might vary with fragment internal excitation, the true shape of the mass 26 derived $P(E_T)$ which is used to separate the contribution of I^* and I in the total $P(E_T)$ distribution could be slightly different from the one which we found. The effect of internal excitation on ionization cross section has been observed in the multiphoton dissociation of ethyl vinyl ether,[25] but its magnitude is not easily obtainable.

Finally, we can compare the fraction of the available energy that went into translation for the two wavelengths. The results are summarized in the following table:

Wavelength	$\langle E_T^* \rangle / E_{avl}^*$	$\langle E_T \rangle / E_{avl}$
248 nm	.58	.46
266 nm	.57	.46

IV. DISCUSSION

A. Anisotropy and polarization

In the two experiments presented here, the anisotropy parameter β is approximately equal to 1.8 regardless of whether I or I^* is formed. Assuming dissociation is fast compared to a rotational period and neglecting vibrations,[17b] $\beta = 2$ when the transition moment lies along the bond dissociation coordinate (parallel transition) and $\beta = -1$ when the transition moment and the bond dissociation coordinate are at 90° (perpendicular transition). Evidently, the processes which we observed are indicative of nearly parallel transitions along the C-I bond.

The question of why β is 1.8 and not 2.0 merits further attention. Considering a truly parallel transition, if the lifetime of the excited state were long enough to allow slight rotation during the dissociation, β would be less than 2. Rotational as well as vibrational motion of the parent could impart a velocity component which is perpendicular to the axial velocity of recoil, thus lowering β. In addition, a transition moment which is not quite parallel to the C-I bond could account for the lower value of β. Finally, β would be lowered if the repulsive force were not operating exactly along the original C-I bond direction during dissociation. In order to assess whether molecular rotation is the cause of an anisotropy parameter of less than 2, we performed an experiment at 266 nm, similar to the ones described here, on the photodissociation of CH_3I. The anisotropy parameter was found to be exactly 2.0 (for both I and I^* channels). Because of the symmetry of this system, the transitions should be either purely parallel or purely perpendicular, and β could only be slightly different from 2 or -1 if the dissociation were affected by rotation or

vibration. Since $\beta = 2.0$, these effects must not be important. In view of the fact that the beam of CH_2ClCH_2I (and of CH_3I) is produced by a supersonic expansion using a rare gas carrier, the rotational temperature is expected to be very low (see part B). Therefore, as in the case of CH_3I, the rotational motion of CH_2ClCH_2I is not expected to be important.

The significance of parallel and perpendicular transitions with respect to low electronic states of the hydrogen and alkyl halides has been discussed extensively by Mulliken[1] and others.[10,12,14,26,27] As mentioned in the Introduction, ground state iodine should be formed by a transition from the ground N state to the $^3Q_1$ or ^1Q states, which would be polarized perpendicular to the C-I bond, while the excited state iodine channel should be correlated to a transition to the $^3Q_0$ state, which would be polarized parallel to the C-I bond. The three of these overlapping Q states together are responsible for the characteristic $n \rightarrow \sigma^*$ absorption continuum of alkyl halides seen in the UV. The fact that we see only a parallel polarization dependence for both I and I^* formation can be explained by assuming the exclusive absorption to $^3Q_0$ and the significant probability of subsequent curve crossing to the $^3Q_1$ or the ^1Q state. The observation of different I^*/I branching ratios at 248 and 266 nm is not surprising because the extent of curve crossing is no doubt a function of excitation energy. In fact, based on the MCD results of Gedanken and Rowe[14] for CH_3I, it is reasonable to assume that excitation at a much higher energy part of the continuum would result in absorption to the ^1Q state in addition to the $^3Q_0$ state, yielding not only a different branching ratio, but a complicated combination of polarization dependences due to curve crossing from $^3Q_0$ to ^1Q and vice versa. We were limited in our experiment by current lasers, so we could only

study the photodissociation process at two wavelengths, but when a tunable UV laser of sufficient power becomes available, it would be instructive to study the photodissociation of an alkyl iodide as a function of excitation energy. Such a study in combination with an MCD investigation should reveal information about the underlying structure of the $n \rightarrow \sigma^*$ continuum and the probability of curve crossing at various excitation energies.

B. Thermochemistry

Our data provides a direct measurement of the energy necessary to break both the C-I and C-Cl bonds in 1,2-chloroiodoethane (assuming no exit channel barrier for C_2H_4Cl decomposition[24,28]). The major error in our reported ΔH for reaction (5) is the uncertainty in the fits to the TOF distributions at mass 26, where a long counting time is required and we only have data at one angle. In order to obtain an accurate value, the fits to the slow side of the mass 26 TOF's must be reliable. The fact that the 248 nm experiment and the 266 nm experiment yield slightly different numbers (see Section III, part B) warrants a detailed comparison of the two experiments. The uncertainty in the low translational energy side of the $P(E_T)$ distribution for each experiment can be seen in the shaded areas in Fig. 11, which correspond to the shaded regions of Figs. 8 and 9. Of course the uncertainties in the entire fits to the mass 26 TOF's will be comparable to that shown in the slow tails, but only the low translational energy threshold is of consequence in determining the total C-I plus C-Cl bond energy. In both experiments, the uncertainty in the fit represents about a 2 kcal/mole uncertainty in the threshold. Thus, the ranges of the two uncertainties overlap

slightly. Nevertheless, we will not average the results of the two experiments, but rather, we will take the lower value, 76.5 ± 1 kcal/mole. The reason for our choice is as follows: because of the decreased temporal resolution due to the high velocity of the molecular beam in the 248 nm experiment and the relatively poor method in which we measured the beam velocity (holeburning), the molecular beam velocity used in the fits could easily be in error by 2%, which could shift the $P(E_T)$ distribution up to 1.5 kcal/mole. (The shaded area in Fig. 11 illustrates the error assuming a well known molecular beam velocity distribution.) In addition to the uncertainty in the beam velocity, the fact that the angular distribution could not be fit exactly makes suspect the use of the 248 nm experimental conditions to derive an energy accurate to ± 1 kcal/mole. In contrast, the 266 nm experiment was performed with a slow, carefully calibrated molecular beam, allowing good temporal resolution in the TOF data. The total error in the $P(E_T)$ due to the uncertainty in the beam velocity for this experiment should be no more than 0.5 kcal/mole. Therefore, the major uncertainty in the $P(E_T)$ is simply the statistical counting error.

Another possibility for error in the determination of the low energy threshold for the mass 26 derived $P(E_T)$ must be considered: the effect of the initial internal energy in the CH_2ClCH_2I parent. Since there are very few low frequency modes (<700 cm^{-1}) in the parent, and since these modes will be partially relaxed in the expansion, the vibrational energy distribution will be roughly exponential with the maximum probability in the ground vibrational state.

If all the modes in the molecule were relaxed to their ground vibrational energy levels, the energy available (E^*_{avl}) would be well defined, and the $P(E_T)$ distribution obtained from the chloroethyl fragment would rise almost vertically from the minimum translational (maximum internal) energy allowed to the C_2H_4Cl radical. On the other hand, if the CH_2ClCH_2I parent were vibrationally excited, then E^*_{avl} would be raised by that amount of excitation. As the difference between E^*_{avl} and the point at which stable C_2H_4Cl radicals are observed is constant (i.e., the C-Cl bond energy of the radical), an increase in E^*_{avl} due to vibrational excitation of the parent must result in a shift toward higher energy in the position of the low translational energy threshold for the $P(E_T)$ obtained from the chloroethyl fragment. Because there is a maximum probability of all the parent molecules in the ground vibrational state, the observed threshold in the $P(E_T)$ will not be affected by E^P_{int}.

The distribution of vibrational energies will, however, change the shape of the $P(E_T)$ in the region of the threshold. The non-vertical rise which we observe can be explained by assuming that the shape of the $P(E_T)$ distribution is unchanged when E^*_{avl} is increased (in other words, assuming the net effect of the Franck-Condon factors is not altered when starting from higher vibrational levels). The entire $P(E_T)$ curve will then be shifted up in energy. The net result is a $P(E_T)$ distribution which is a convolution of $P(E_T)$ curves which arise from and are weighted by the vibrational energy distribution in the CH_2ClCH_2I parent. Hence, the low energy side of the mass 26 derived $P(E_T)$ will rise more gently than would be expected if all the parent modes were relaxed.

Rotational excitation will not be very important because of the efficient rotational cooling in the molecular beam. The rotational temperature can be estimated by assuming it is equal to the terminal longitudinal translational temperature in the beam, which is related to the α parameter in the form for the velocity distribution (see Section II) by[23]

$$\alpha = \left(\frac{2kT}{m}\right)^{1/2} . \qquad (6)$$

For the experiment at 266 nm, $T \cong 4$ K, and at 248 nm, $T \cong 3$ K. These temperatures correspond to negligible rotational energies.

One final consideration in the calculation of the C-I plus C-Cl bond energy is whether or not secondary dissociation occurs on a time scale short compared to the flight time from the interaction region to the ionizer. Using chloroethyl frequencies from Schlegel,[24] moments of inertia and activated complex frequencies estimated by Skinner and Rabinovitch,[28] and a C-Cl bond energy of 20 kcal/mole, we performed an RRKM calculation. The calculated lifetime of the chloroethyl radical with only 0.1 kcal/mole above the dissociation limit is $< 10^{-8}$ sec, while the flight time to the ionizer is $\sim 10^{-4}$ to 10^{-5} sec. Consequently, there will be no possibility that any radical with more internal energy than $D_0^0(C_2H_4\text{-}Cl)$ could survive to be counted.

Given our result of 76.5 ± 1 kcal/mole for the ΔH at 0 K of reaction (5), the heat of formation $\Delta H_f^0(0)$ of 1,2-chloroiodoethane follows directly (refer to Table II): $\Delta H_{f,0}^0(CH_2ClCH_2I) = -7.8 \pm 1$ kcal/mole. Using the method of group contributions,[29,30] the heat of formation of CH_2ClCH_2I can be estimated by adding $1/2[\Delta H_{f,0}^0(CH_2ClCH_2Cl)]$ and $1/2[\Delta H_{f,0}^0(CH_2ICH_2I)]$ to give -3.7 kcal/mole. Even in the limits of accuracy in the reported heats of

formation, the two results disagree by about 2 kcal/mole. Because of the sparsity of thermochemical data on the 1,2-dihaloethanes containing two different halogens, the group contribution method of calculating ΔH_f^o's has not been tested very thoroughly. A 2-4 kcal/mole discrepancy between theory and experiment could be quite reasonable.

If the C-I bond energy of 1,2-chloroiodoethane were known, it would be a simple matter to obtain the C-Cl bond energy of the chloroethyl radical from our experimental results. $D_o^o(CH_2ClCH_2\text{-}I)$ can be estimated roughly by studying the changes in the heats of formation in the following scheme:

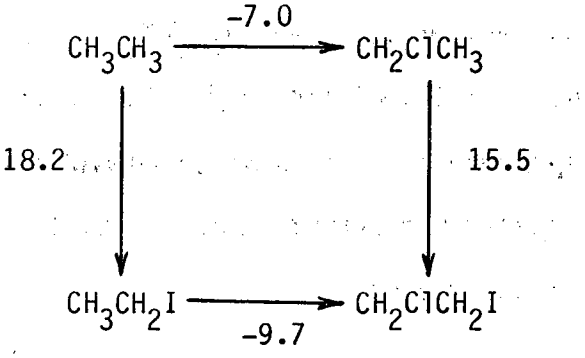

The numbers shown are the changes in $\Delta H_f^o(0)$ for each step in units of kcal/mole. It is seen that CH_2ClCH_2I is 2.7 kcal/mole more stable than we would predict assuming simple bond additivity in the heats of formation. This added stability of the molecule probably manifests itself in the increased bond energy of the C-Cl, C-C, and C-I bonds, though the distribution of the energy is not clear. Weissman and Benson[31] estimate an increase of 2.5 kcal/mole in the C-C bond energy on going from CH_3CH_3 to CH_3CH_2Cl, and from CH_3CH_3 to CH_2ClCH_2Cl, they report an increase of 2.8 kcal/mole in the C-C bond energy. These numbers, while illustrating the chlorine substitution effect, are subject to errors of at least ± 1 kcal/mole. For our pur-

pose, we will assume an increase of 1 kcal/mole in $D^o_0(CH_2ClCH_2-I)$ over $D^o_0(CH_3CH_2-I)$. The result is a C-I bond energy for 1,2-chloroiodoethane of 55.3 ± 1 kcal/mole (at 0 K), leading to: $D^o_0(C_2H_4-Cl)$ = 76.5 - 55.3 = 21.2 ± 2 kcal/mole and $\Delta H^o_{f,0}(C_2H_4Cl)$ = 21.9 ± 2 kcal/mole.

A comparison can be made with the chloroethyl radical heat of formation which we estimate and the $\Delta H^o_{f,0}(C_2H_4Cl)$ derived by different methods. Assuming $D^o_0(CH_3CH_2-H) = D^o_0(CH_2ClCH_2-H)$, then $\Delta H^o_{f,0}(C_2H_4Cl)$ is calculated from data in Table II to be 23.6 ± 1 kcal/mole. Schlegel and Sosa[24] have performed an ab initio calculation for the reaction of Cl with C_2H_4, where they report a theoretical value of 19.5 ± 2 kcal/mole for the C-Cl bond energy of the chloroethyl radical at 0 K, corresponding to a $\Delta H^o_{f,0}(C_2H_4Cl)$ of 23.6 ± 2 kcal/mole. Within the reported limits of accuracy, all the values agree. However, since bond dissociation energies in many chlorinated ethanes depend on the heat of formation of the 2-chloroethyl radical, it will be advantageous to narrow the limits of uncertainty.

ACKNOWLEDGEMENTS

This work was supported by the Director, Office of Energy Research, Office of Basic Energy Sciences, Chemical Sciences Division of the U.S. Department of Energy under Contract No. DE-AC03-76SF00098. The excimer laser was on loan from the San Francisco Laser Center, a National Science Foundation Regional Instrumentation Facility, NSF Grant No. CHE79-16250 awarded to the University of California at Berkeley in collaboration with Stanford University. We are grateful for discussions with Professors Sidney Benson and H. Bernhard Schlegel. P. F. thanks the Swiss National Foundation for his postdoctoral fellowship.

REFERENCES

1. (a) R. S. Mulliken, Phys. Rev. 50, 1017 (1936); (b) 51, 310 (1937); (c) 47, 413 (1935); (d) J. Chem. Phys. 8, 382 (1940).
2. R. A. Boschi and D. R. Salahub, Mol. Phys. 24(2), 289 (1972).
3. D. Porret and C. F. Goodeve, Proc. Roy. Soc. A 165, 31 (1938).
4. J. V. V. Kasper and G. C. Pimentel, Appl. Phys. Lett. 5, 231 (1964).
5. (a) J. V. V. Kasper, J. H. Parker, and G. C. Pimentel, J. Chem. Phys. 43, 1827 (1965); (b) M. A. Pollack, Appl. Phys. Lett. 8, 36 (1966).
6. D. Husain and R. J. Donovan, Adv. Photochem. 8, 1 (1971).
7. M. Dzvonik, S. Yang, and R. Bersohn, J. Chem. Phys. 61(11), 4408 (1974).
8. S. Riley and K. Wilson, Discuss. Faraday Soc. 53, 132 (1972).
9. R. K. Sparks, K. Shobatake, L. R. Carlson, and Y. T. Lee, J. Chem. Phys. 75(8), 3838 (1981).
10. Douglas J. Krajnovich, Ph.D. thesis, University of California, Berkeley, 1983.
11. D. J. Krajnovich, L J. Butler, and Y. T. Lee (to be published in J. Chem. Phys.).
12. R. D. Clear, S. J. Riley, and K. R. Wilson, J. Chem. Phys. 63(4), 1340 (1975).
13. R. J. Oldman, R. K. Sander, and K. R. Wilson, J. Chem. Phys. 54, 4127 (1971).
14. A. Gedanken and M. D. Rowe, Chem. Phys. Lett. 34(1), 39 (1975).
15. G. E. Busch, J. F. Cornelius, R. T. Mahoney, R. I. Morse, D. W. Schlosser, and K. R. Wilson, Rev. Sci. Instr. 41, 1066 (1970).

16. K. R. Wilson, "Photofragment Spectroscopy of Dissociative Excited States," in Chemistry of the Excited State, edited by J. N. Pitts, Jr. (Gordon and Breach, New York, 1970).

17. G. E. Busch and K. R. Wilson, J. Chem. Phys. 56(7), 3626 (1972); (b) 56(7), 3638 (1972).

18. T. F. Hunter, S. Lunt, and K. S. Kristjansson, J. Chem. Soc., Faraday Trans. 2 79, 303 (1983).

19. P. Brewer, P. Das, G. Ondrey, and R. Bersohn, J. Chem. Phys. 79(2), 720 (1983).

20. S. L. Baughcum and S. R. Leone, J. Chem. Phys. 72(12), 6531 (1980).

21. N. Van Veen (Private Communication).

22. Y. T. Lee, J. D. McDonald, P. R. LeBreton, and D. R. Herschbach, Rev. Sci. Instrum. 40, 1402 (1969).

23. R. B. Berstein, Chemical Dynamics via Molecular Beam and Laser Techniques (Oxford University Press, New York, 1982) p. 30.

24. H. B. Schlegel and C. Sosa, 1983 (to be published in J. Phys. Chem).

25. F. Huisken, D. Krajnovich, Z. Zhang, Y. R. Shen, and Y. T. Lee, J. Chem. Phys. 78(6), 3086 (1983).

26. T. Donohue and J. R. Wiesenfeld, J. Chem. Phys. 63(7), 3130 (1975).

27. T. F. Hunter and K. S. Kristjansson, Chem. Phys. Lett. 58(2), 291 (1978).

28. G. B. Skinner and B. S. Rabinovitch, Bull. Soc. Chim. Belg. 82, 305 (1973).

29. S. W. Benson, F. R. Cruickshank, D. M. Golden, G. R. Haugen, H. E. O'Neal, A. S. Rodgers, R. Shaw, R. Walsh, Chem, Rev. 69, 279 (1969).

30. S. W. Benson, Thermochemical Kinetics, 2nd ed. (Wiley, New York, 1976).

31. M. Weissman and S. Benson, J. Phys. Chem. 87, 243 (1983).

32. JANAF Thermochemical Tables, 2nd Ed. Natl. Stand. Ref. Data Ser., U. S. Natl. Bur. Stand. 37 (U. S. Government Printing Office, Washington D. C., 1971).

33. S. W. Benson, J. Chem. Ed. 42(9), 502 (1965).

34. A. L. Castelhano, P. R. Marriott, and D. Griller, J. Am. Chem. Soc. 103, 4262 (1981).

35. S. W. Benson and A. Amano, J. Chem. Phys. 36(12), 3464 (1962).

36. J. R. Lacher, A. Amador, and J. D. Park, Trans. Faraday Soc. 63, 1608 (1967).

37. J. Chao, A. S. Rodgers, R. C. Wilhoit, and B. J. Zwolinski, J. Phys. Chem. Ref. Data 3(1), 143 (1974).

38. J . C. Traeger, R. G. McLoughlin, J. Am. Chem. Soc. 103, 3647 (1981).

TABLE I. $I^*(^2P_{1/2})$ quantum yields for CH_3I photolysis at 266 and 248 nm.

λ(nm)	Φ_I^*	Method	Reference
266	0.70	photofragment spectroscopy	9[a]
266	~0.78	photofragment spectroscopy	8
266	0.77	optoacoustic	18[b]
248	0.81	infrared emission	20
248	0.71	photofragment spectroscopy	21
248	0.59	optoacoustic	18[b]

[a]Taken from translational energy distribution.

[b]Estimated from plot.

TABLE II. Standard molar enthalpies of formation for some substances at 300 K and 0 K.

Species	ΔH_f^o(300 K) (kcal/mole)	ΔH_f^o(0 K) (kcal/mole)	Reference
Cl	28.92±0.03	28.52±0.03	32
H	52.103±0.001	51.631±0.001	32
I	25.53±0.01	25.63±0.01	32
CH_3I	3.4±0.3	5.7±0.3[a]	34
$CH_2{=}CH_2$	12.53±0.07	14.58±0.07	32
CH_3CH_3	-20.08±0.05	-16.33±0.05[a]	38
CH_3CH_2Cl	-26.83±0.18	-23.3±0.2[a]	37
CH_2ClCH_2Cl	-30.2±1	-27.1±1[a]	36
CH_3CH_2I	-2.0±0.4	1.9±0.5[a]	34
CH_2ICH_2I	15.9±0.2	19.7±0.3[a]	35
CH_2ClCH_2I	-11.37±1.2[a]	-7.8±1.0	this work
CH_3	34.4±.4	35.2±0.4	38
CH_3CH_2	28.0±1.0	30.6±1.0[a]	34
CH_2ClCH_2	21.2±1.0[a]	23.6±1.0[b]	estimate

[a]Calculated by correcting for thermal energy.[33]

[b]Calculated assuming $D_o^o(CH_2ClCH_2\text{-}H) = D_o^o(CH_3CH_2\text{-}H)$ (see text).

FIGURE CAPTIONS

Figure 1. Schematic diagram of the center-of-mass velocity distribution for the two recoiling photodissociation products. The shaded area depicts those C_2H_4Cl radicals with slow velocities, or low translational energies, which have enough internal excitation to dissociate into C_2H_4 and Cl. From conservation of momentum, detection of either fragment should yield the total c.m. translational energy distribution. However, because of secondary dissociation of the chloroethyl product, the iodine fragment is monitored to provide the lost information.

Figure 2. Schematic diagram of the experimental apparatus. The numbers correspond to pressures in Torr for the various regions.

Figure 3. Laboratory TOF distrubutions of I atom product at 266 nm for five detector angles. O Experimental points; —— calculated using the $P(E_T)$ in Fig. 12 and $\beta = 1.8$.

Figure 4. Laboratory TOF distributions of I atom product at 248 nm for four detector angles. O Experimental points; —— calculated using the $P(E_T)$ in Fig. 12 and $\beta = 1.8$.

Figure 5. Newton diagram representing photodissociation of CH_2ClCH_2I at 248 nm with detection of iodine. Velocity vectors shown are the molecular beam velocity $\underset{\sim}{V}_b$, the center of mass velocity of the I fragment $\underset{\sim}{V}_{cm}$, and the laboratory velocity of the I fragment $\underset{\sim}{V}_{lab}$. The relevant angles are the c.m. angle θ and the lab. angle Θ.

Figure 6. Laboratory angular distribution of I atom product at 266 nm. ● Experimental points, obtained by integrating and normalizing the TOF distributions in Fig. 3 (except for the point at 35°). ± 2σ error bars are smaller than the symbols. ——— $\beta = 1.8$; — — — $\beta = 1.7$; – – – – $\beta = 1.9$.

Figure 7. Laboratory angular distribution of I atom product at 248 nm. ● Experimental points, obtained by integrating and normalizing many different TOF distributions. ± 2σ error bars are smaller than the symbols. ——— $\beta = 1.8$, — — — $\beta = 1.9$; – – – – $\beta = 2.0$.

Figure 8. Laboratory TOF distribution of all products detected at m/e = 26 at 248 nm for $\Theta = 10°$. Only the experimental points are shown.

Figure 9. Blow-up of the region including the spike in Fig. 8. The peak here arises from the m/e = 26 fragment of the stable C_2H_4Cl radicals. O Experimental points; ——— best fit calculated using the $P(E_T)$ in Fig. 11 and $\beta = 1.8$. The shaded region illustrates the uncertainty in the fit to the slow tail which gives rise to an uncertainty of ± 1 kcal/mole in the low translational energy side of the $P(E_T)$ distribution.

Figure 10. Laboratory TOF distribution of C_2H_4Cl product (detected at m/e = 26) at 266 nm for $\Theta = 7^\circ$. O Experimental points; ——— best fit calculated using the $P(E_T)$ in Fig. 11 and $\beta = 1.8$. The shaded region illustrates the uncertainty in the fit to the slow tail which gives rise to an uncertainty of ± 1 kcal/mole in the low translational energy side of the $P(E_T)$ distribution.

Figure 11. Laboratory TOF distribution of products detected at m/e = 35 at 248 nm for $\Theta = 10^\circ$. Only experimental points are shown.

Figure 12. C.M. Recoil translational energy distributions for 1,2-chloroidoethane photodissociation at 248 and 266 nm. ——— Total $P(E_T)$ derived from fitting TOF's of iodine fragment. — — — Derived from measurement of C_2H_4Cl fragment; with the exception of the low translational energy section, this curve corresponds to formation of $I^*(^2P_{1/2})$ because $I(^2P_{3/2})$ formation leads to complete secondary dissociaton of the radical. — — — — $P(E_T)$ for I^* subtracted from total $P(E_T)$, giving the $P(E_T)$ for ground state I formation. E_{avl} is the excess energy after breaking the C-I bond in CH_2ClCH_2I. E^*_{avl} is E_{avl} minus the I atom spin-orbit excitation (21.7 kcal/mole). Total fragment internal energy is given by E_{avl} (or E^*_{avl}) minus the c.m. translational energy. The shaded areas show the uncertainty in the low energy side of the $P(E_T)$ derived from mass 26 TOF data, which arises from the uncertainty in the fits to the slow tails in Figs. 8 and 9. The resulting uncertainty in the low energy thresholds of the $P(E_T)$'s is ± 1 kcal/mole.

Figure 13. Energy level diagram for the photodissociation of CH_2ClCH_2I at 248 and 266 nm.

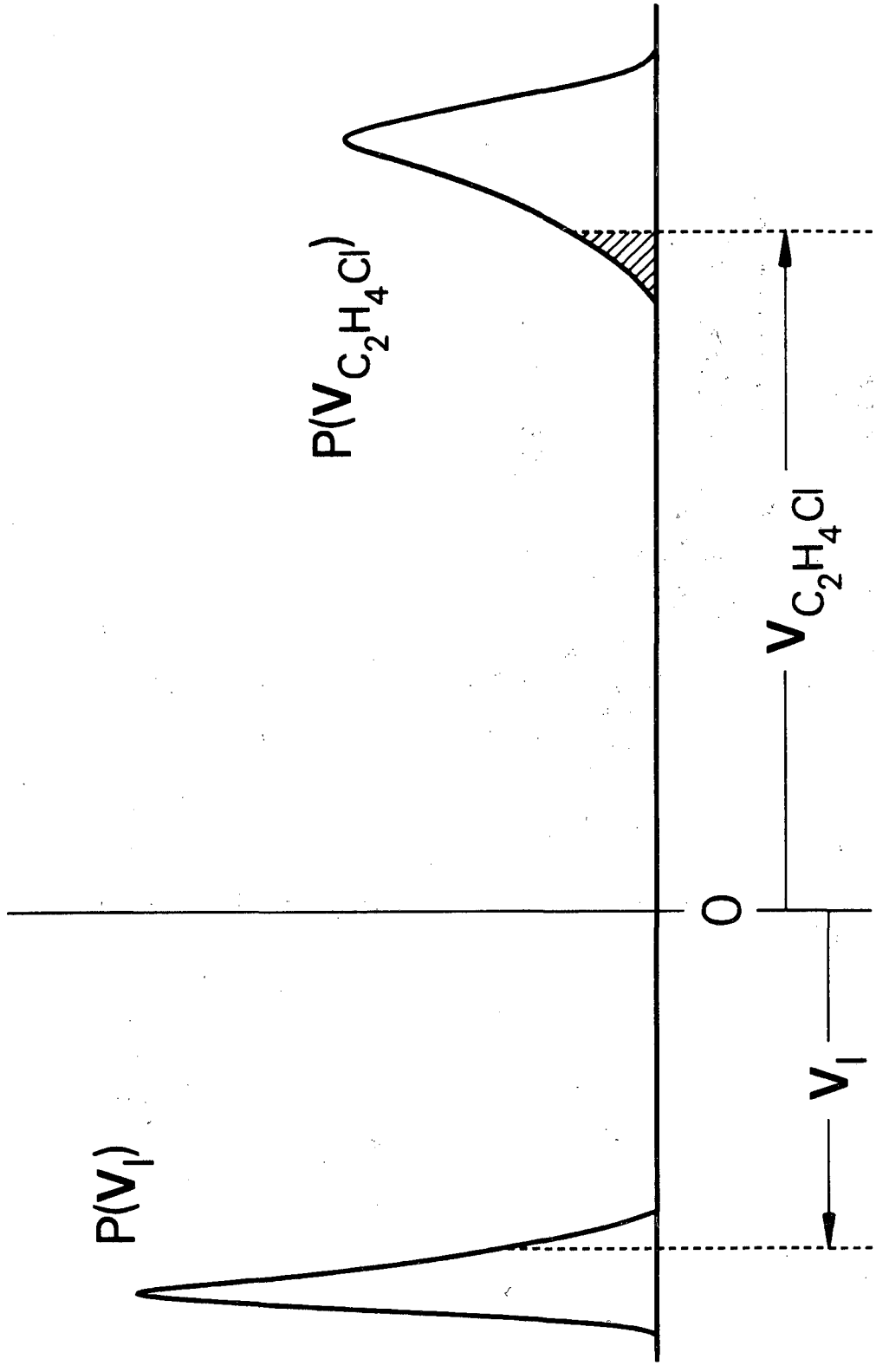

XBL 844-1394

Fig. 1

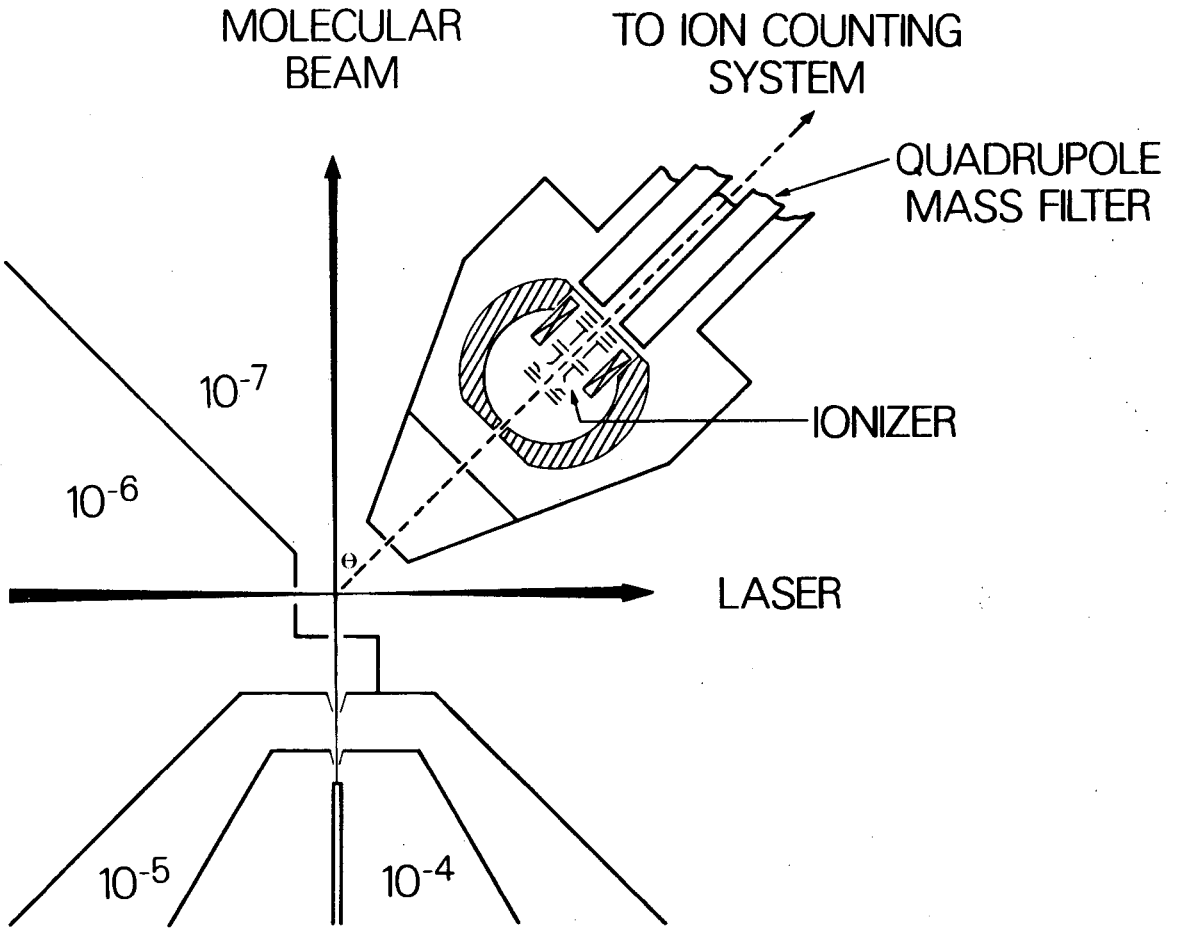

XBL 844-1401

Fig. 2

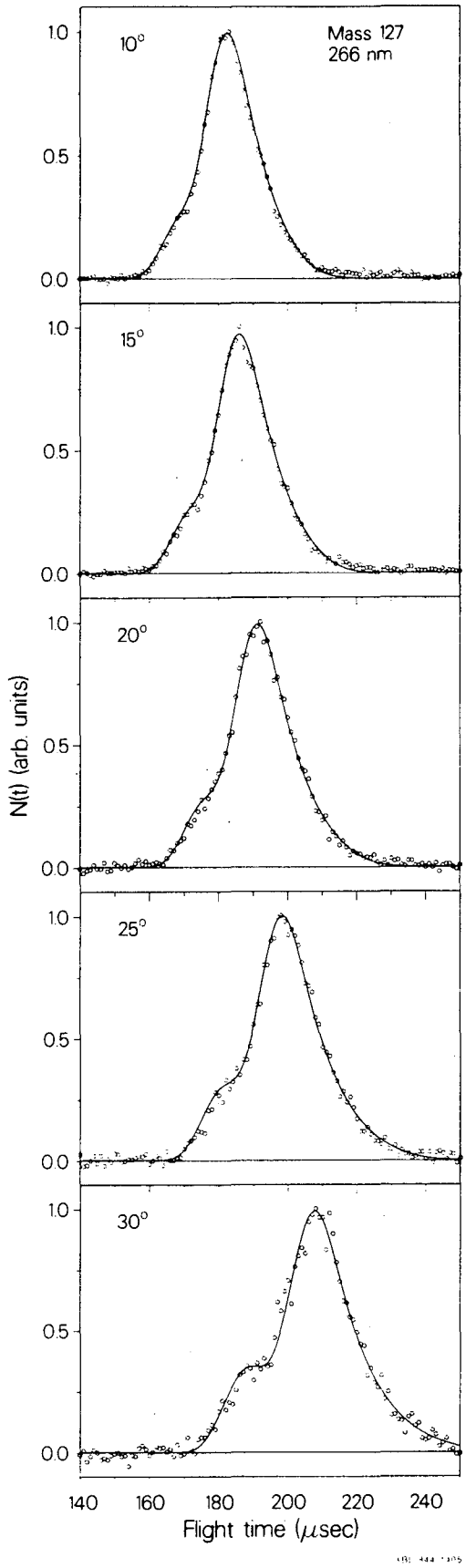
Mass 127
266 nm
10°
15°
20°
25°
30°
1.0
0.5
0.0
N(t) (arb. units)
140
160
180
200
220
240
Flight time (μsec)

Fig. 3

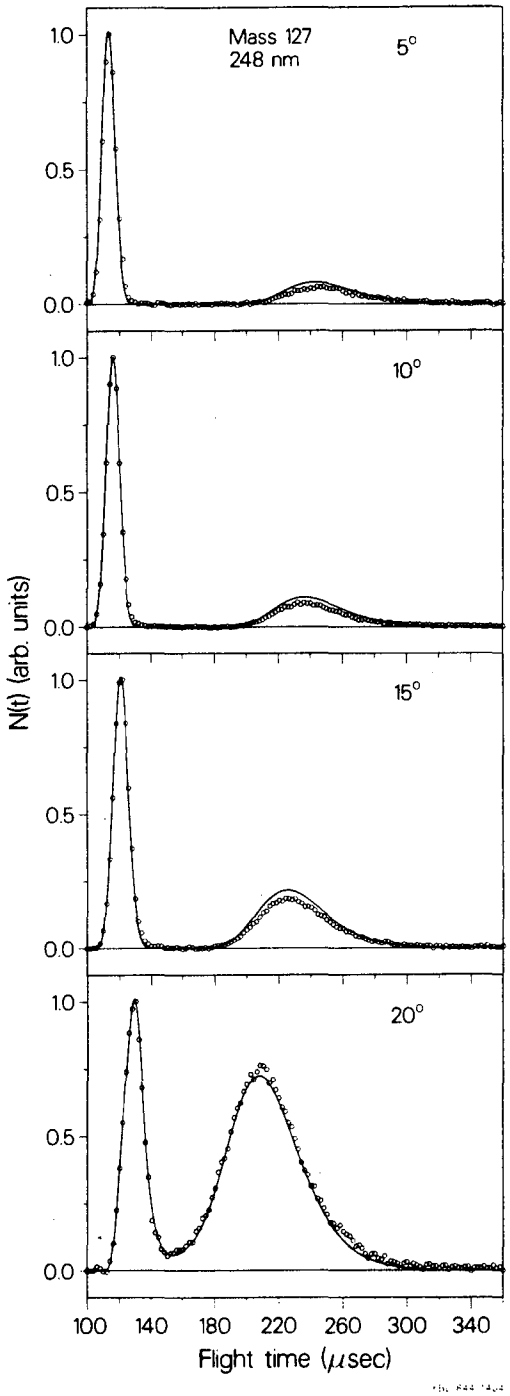
Mass 127
248 nm
5°
10°
15°
20°
1.0
0.5
0.0
N(t) (arb. units)
100
140
180
220
260
300
340
Flight time (μsec)

Fig. 4

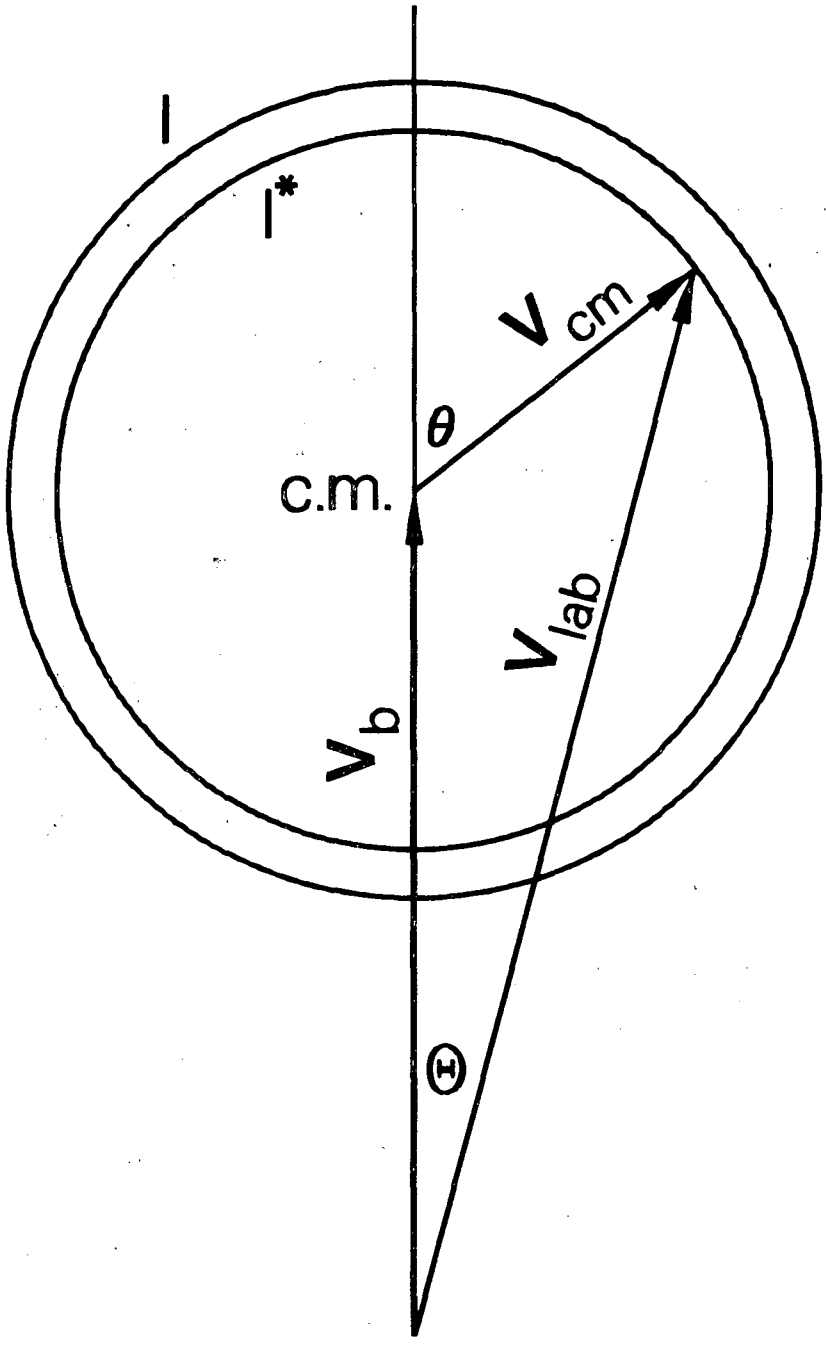

XBL 844-1402

Fig. 5

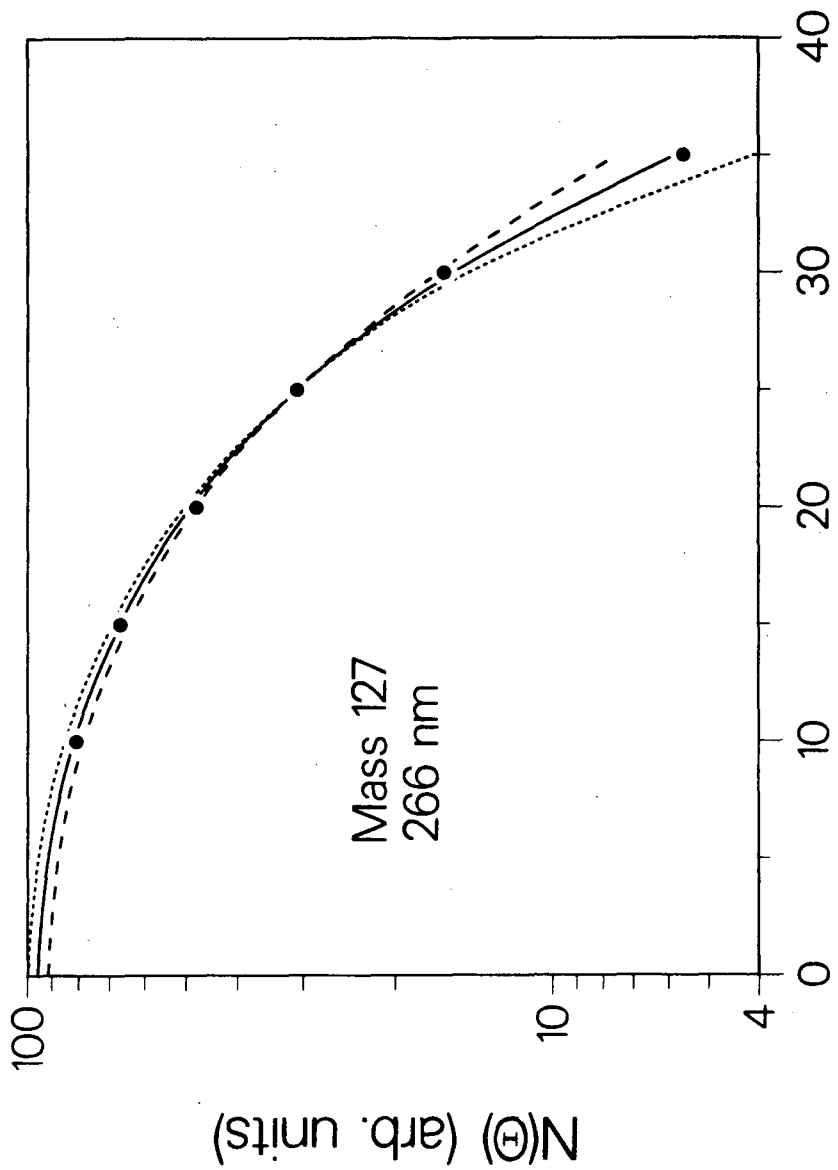
N(Θ) (arb. units)
100
10
4
0
10
20
30
40
Lab. angle (deg)
Mass 127
266 nm
XBL 844-1396

Fig. 6

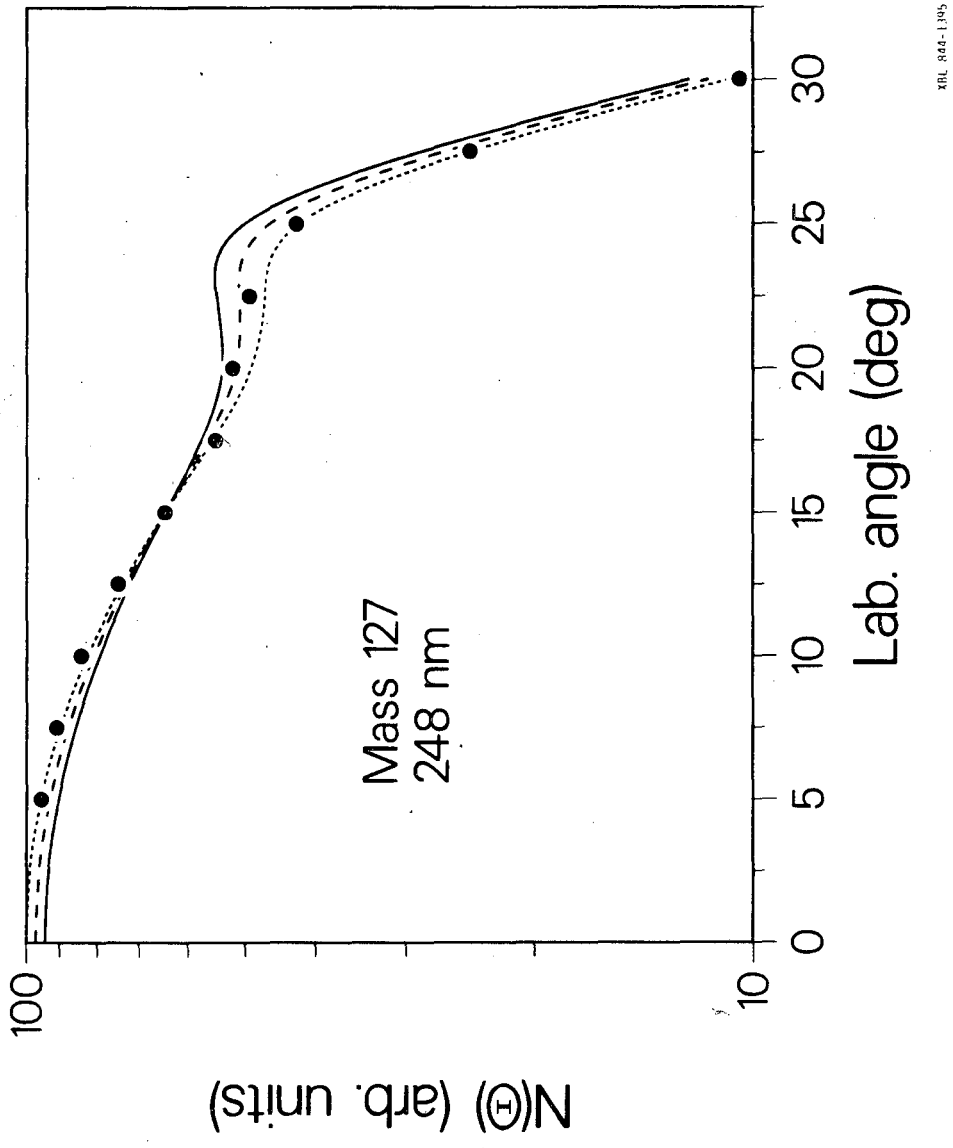
N(Θ) (arb. units)
100
10
0
5
10
15
20
25
30
Lab. angle (deg)
Mass 127
248 nm
XBL 844-1395

Fig. 7

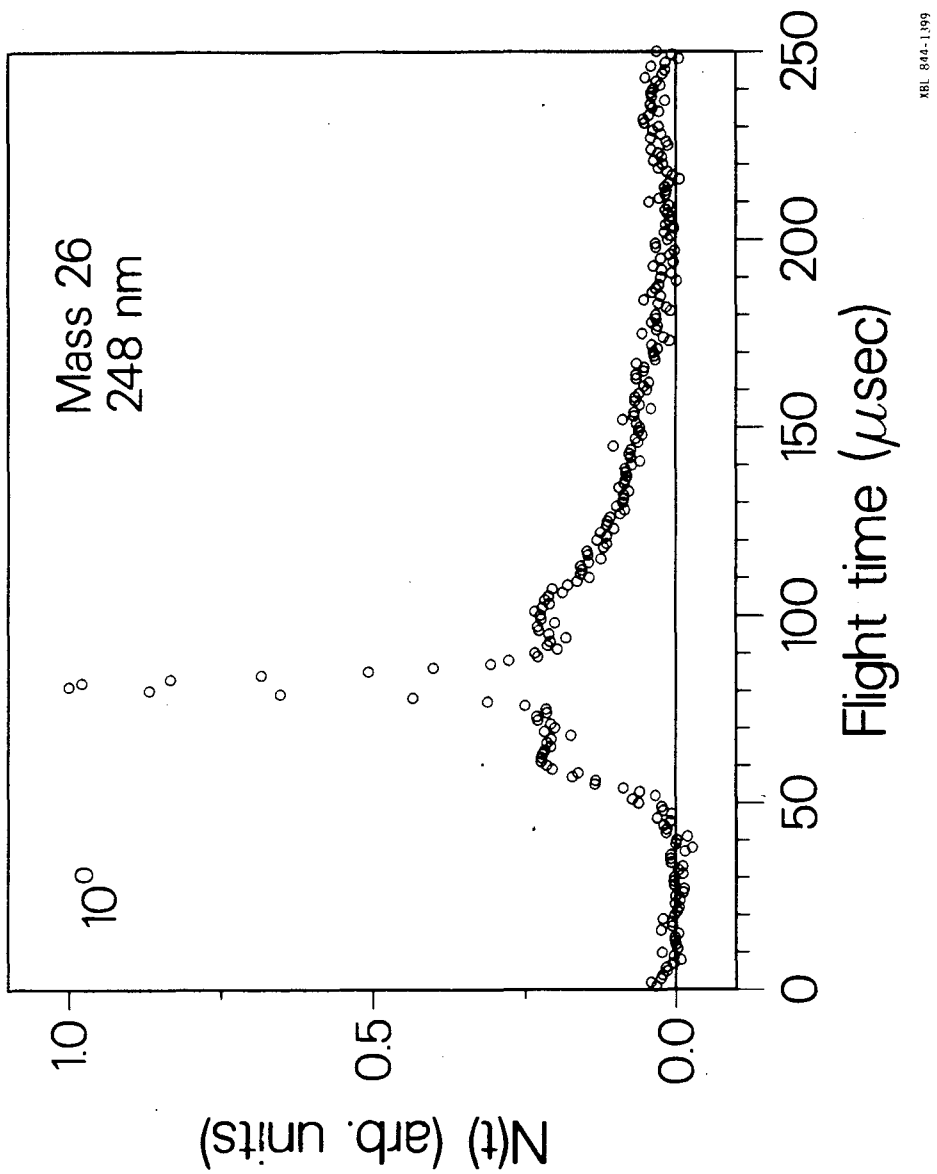

XBL 844-1199

Fig. 3

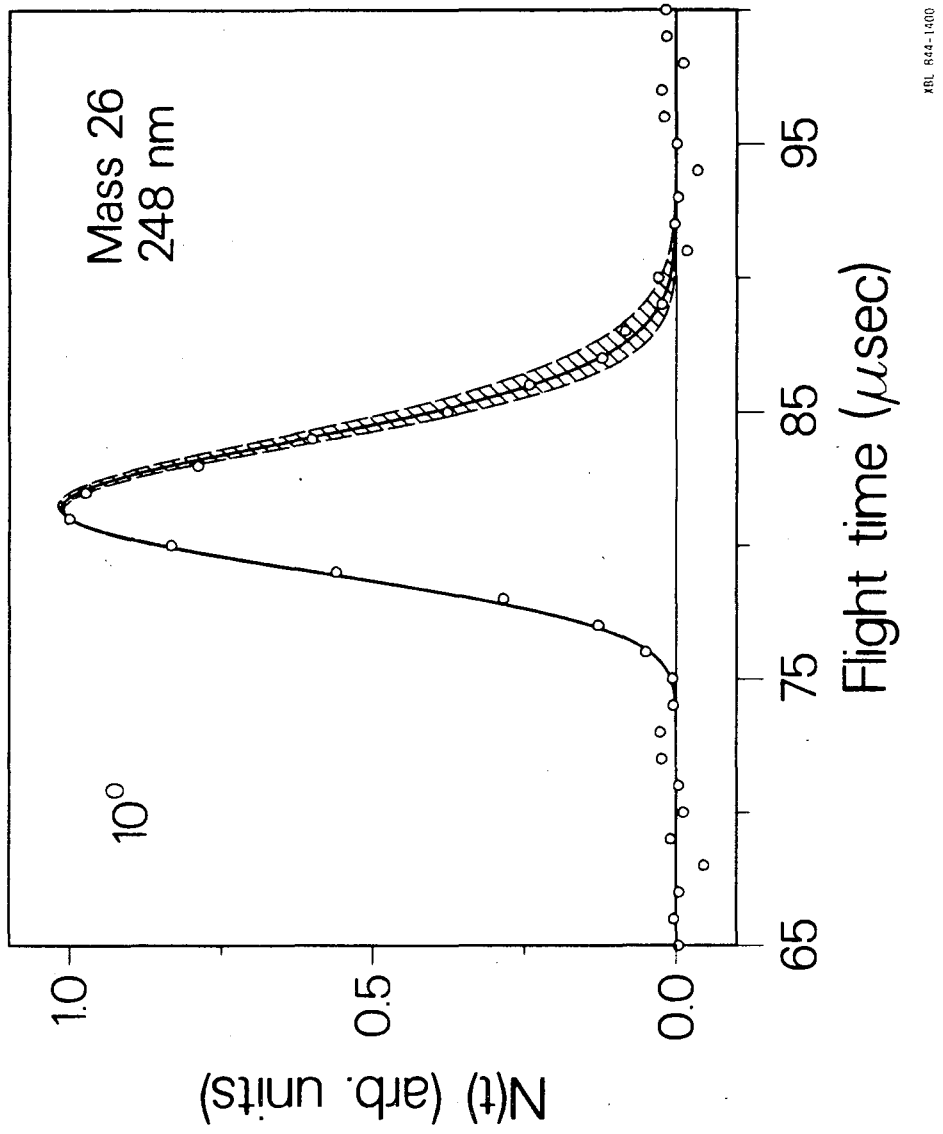
Mass 26
248 nm
10°
N(t) (arb. units)
1.0
0.5
0.0
65
75
85
95
Flight time (μsec)
XBL 844-1400

Fig. 9

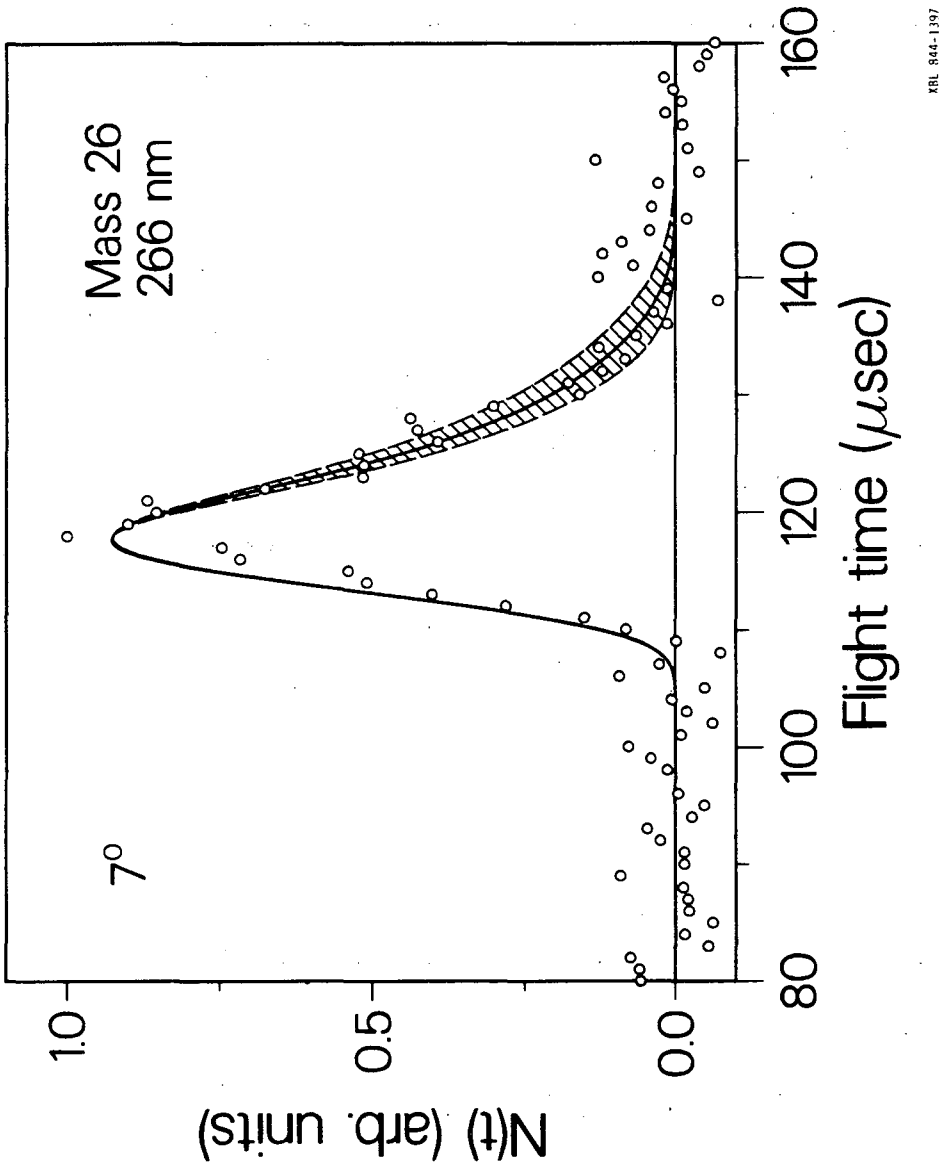
Mass 26
266 nm
7°
N(t) (arb. units)
1.0
0.5
0.0
80
100
120
140
160
Flight time (μsec)
XBL 844-1397

Fig. 10

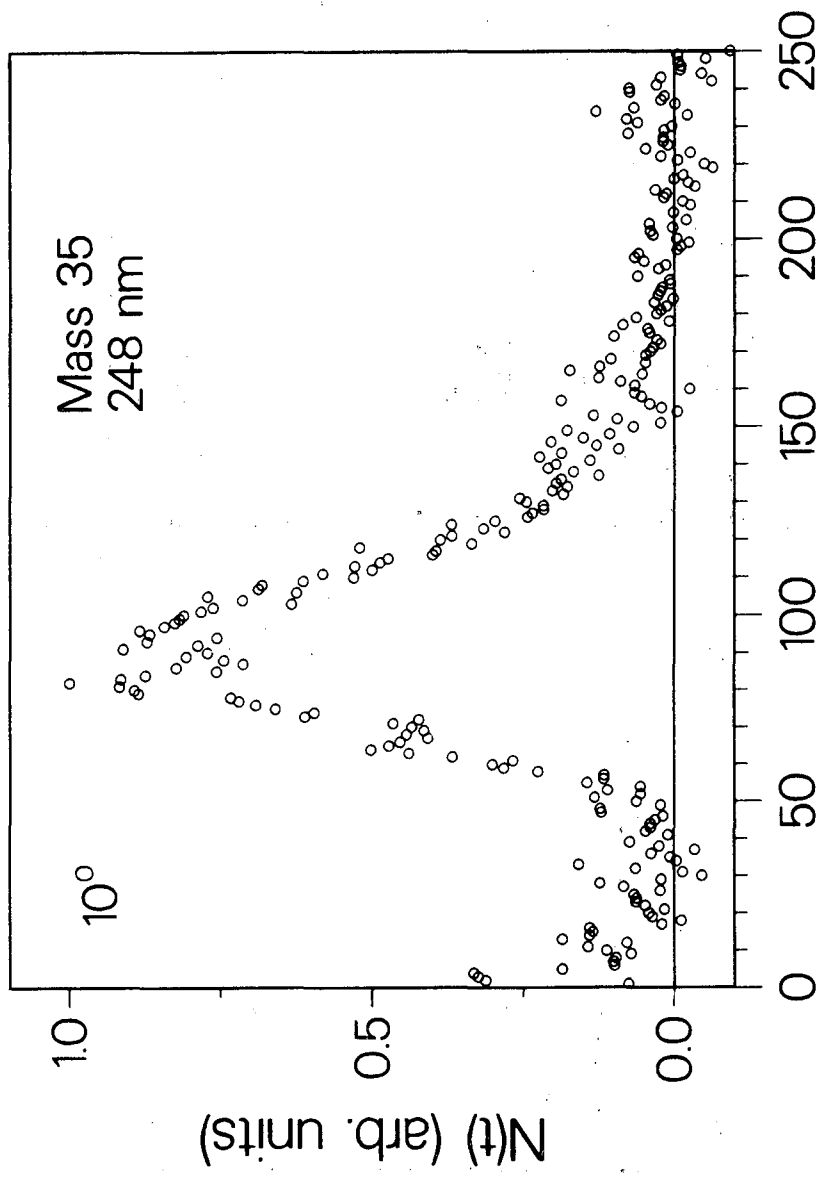
Mass 35
248 nm
10^0
N(t) (arb. units)
1.0
0.5
0.0
0
50
100
150
200
250
Flight time (μsec)
XBL 844-1398

Fig. 11

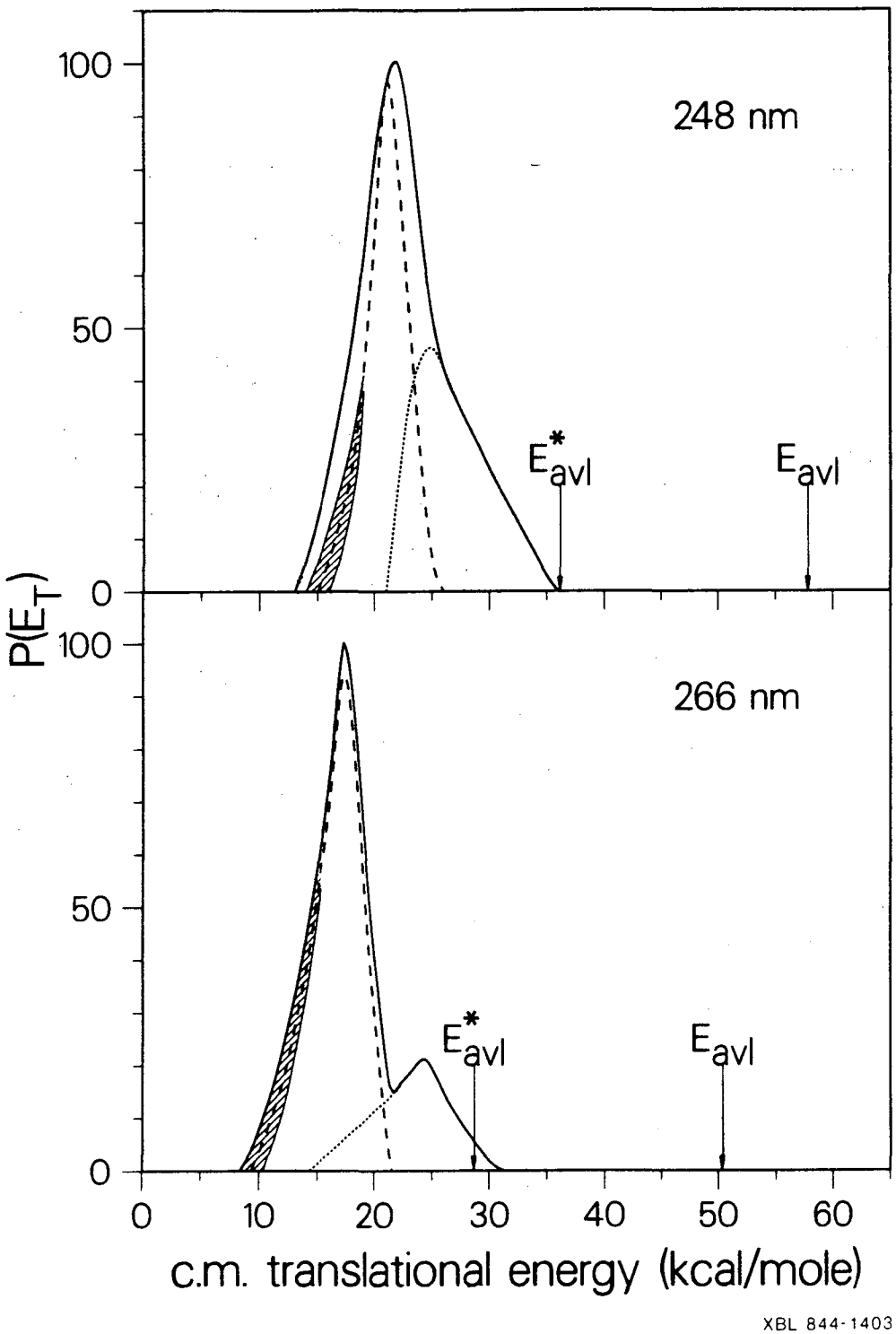
100
50
0
248 nm
E^*_{avl}
E_{avl}
$P(E_T)$
100
50
0
266 nm
E^*_{avl}
E_{avl}
0
10
20
30
40
50
60
c.m. translational energy (kcal/mole)
XBL 844-1403

Fig. 12

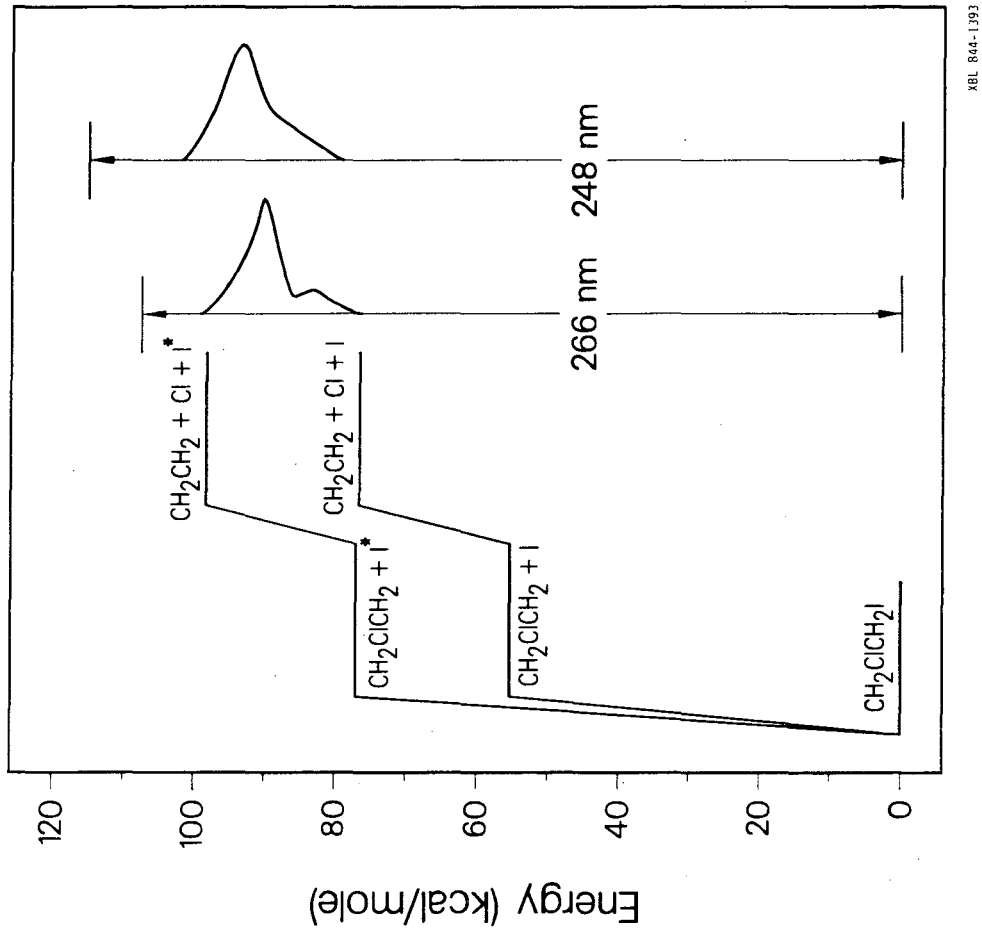
Energy (kcal/mole)
120
100
80
60
40
20
0
$CH_2CH_2 + Cl + I^*$
$CH_2CH_2 + Cl + I$
$CH_2ClCH_2 + I^*$
$CH_2ClCH_2 + I$
CH_2ClCH_2I
266 nm
248 nm
XBL 844-1393

Fig. 13

TECHNICAL INFORMATION DEPARTMENT
LAWRENCE BERKELEY LABORATORY
UNIVERSITY OF CALIFORNIA
BERKELEY, CALIFORNIA 94720